Imaging subducted slab structure beneath the Sea of Okhotsk with teleseismic waveforms

Zhongwen Zhan, Donald V. Helmberger, Dunzhu Li

Supplementary Figures

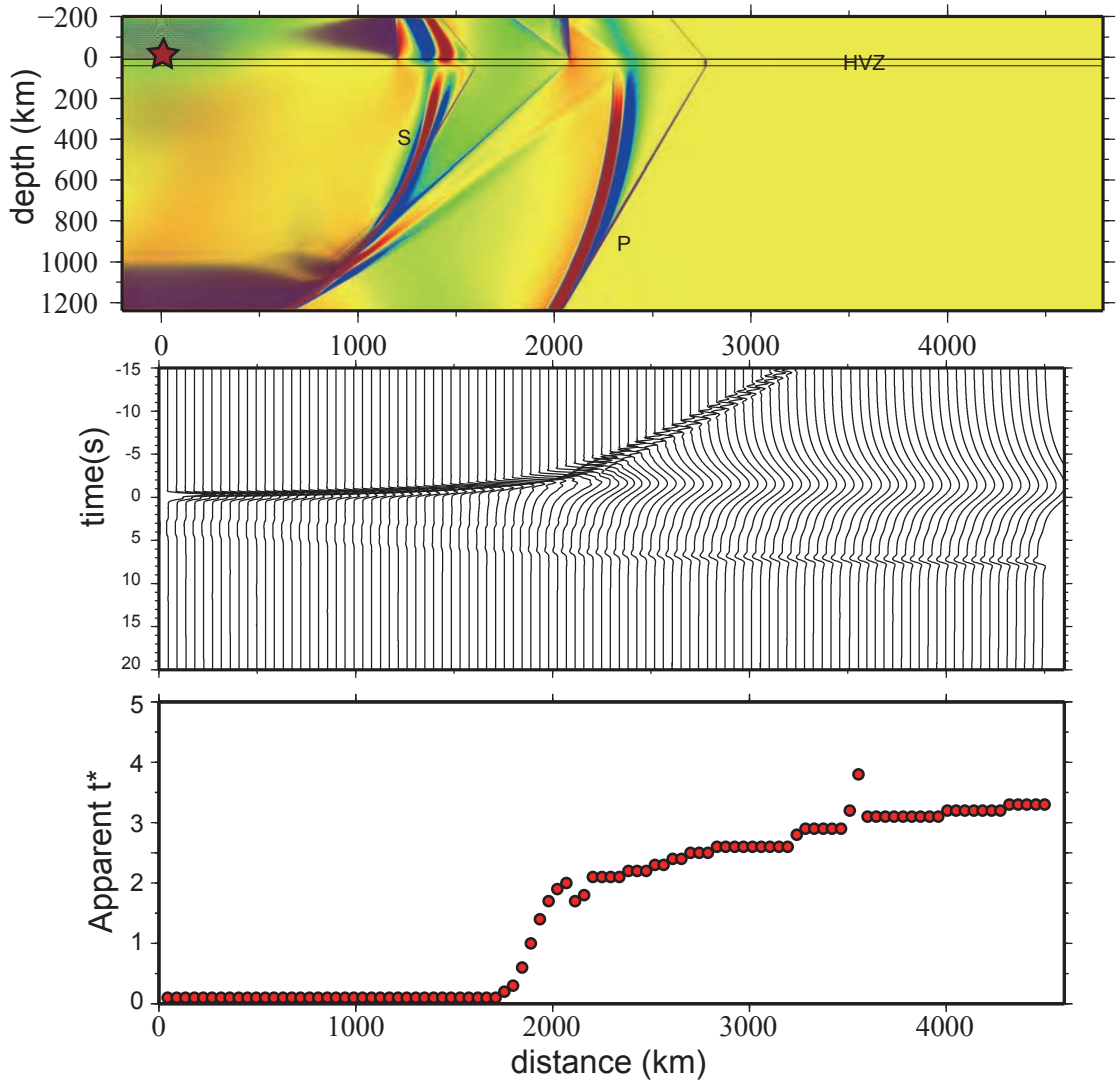

Figure S1. Examples of elastic tunneling effect by a high-velocity slab. We assume a homogeneous lower half space with Vp = 8km/s with a uniform slab 15% higher in velocity and with a thickness of 30 km. An explosive source is located near the top edge of the high-velocity slab, shown as the red star. The top panel displays the snapshot of the velocity field. Receivers are located at the bottom and their synthetics are displayed in the middle panel. The high-velocity layer has little effect before critical angle is reached near a distance of 1600 km. Three P-wave arrivals appear at larger distance; the first travels along the slab as a plate-wave before diffracting to the receivers; the second is the tunneled phase, and the third is diffracted at the shadow-edge (critical angle point) with a longer path, see Mellman & Helmberger (1974) for analytical details. The tunneled arrival depends on slab thickness and maps into a simulated attenuation operator (t*) as displayed in the lower panel (measured by cross-correlating the P waves with the Futterman functions). Therefore, the waveform effect of this particular slab model is equivalent to a strong attenuation with t* of 2 to 3.

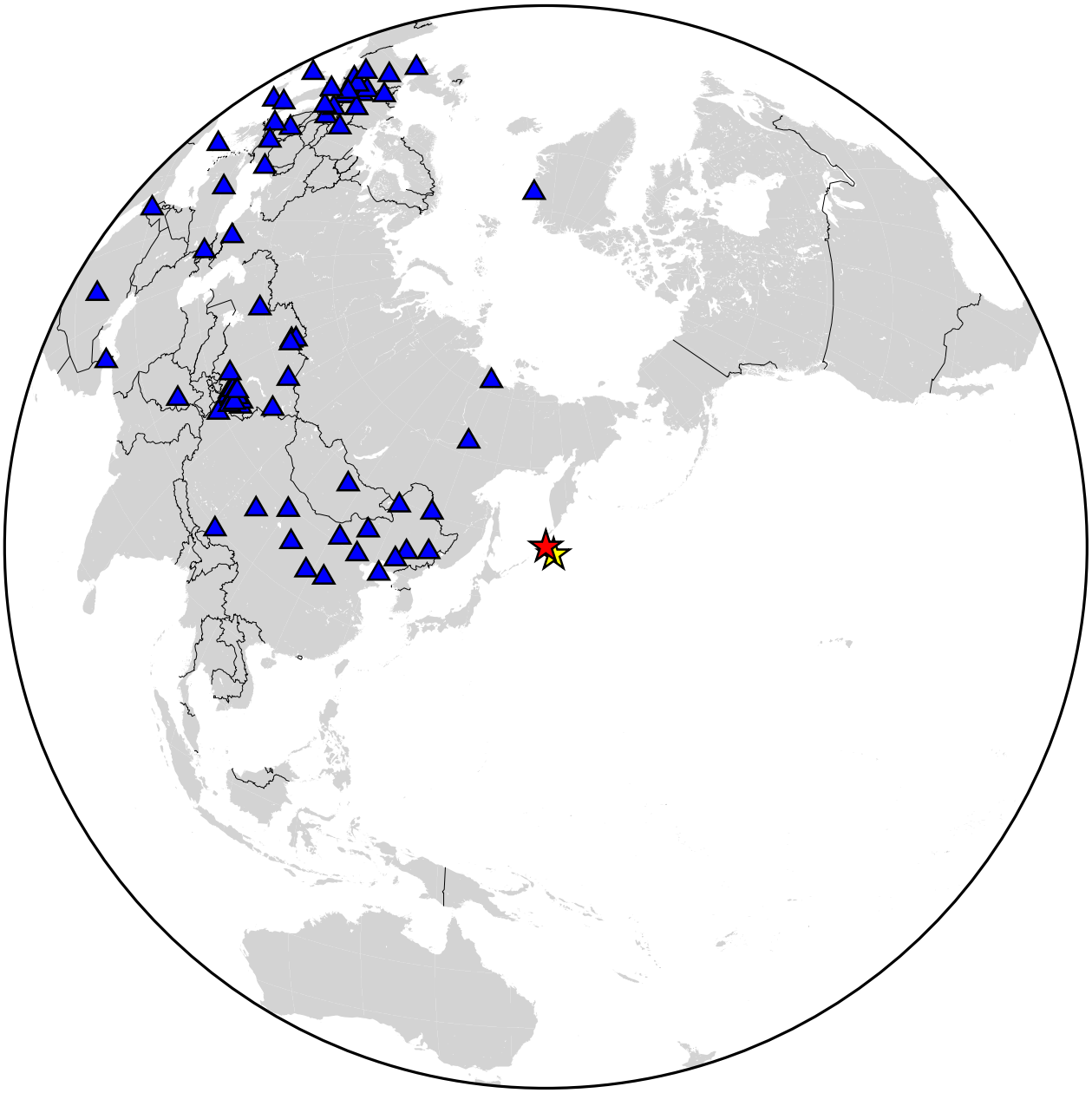

Figure S2. Teleseismic stations used in this study are shown as blue triangles. The red and yellow stars are the 2009 interplate and 2007 outer-rise earthquakes respectively.

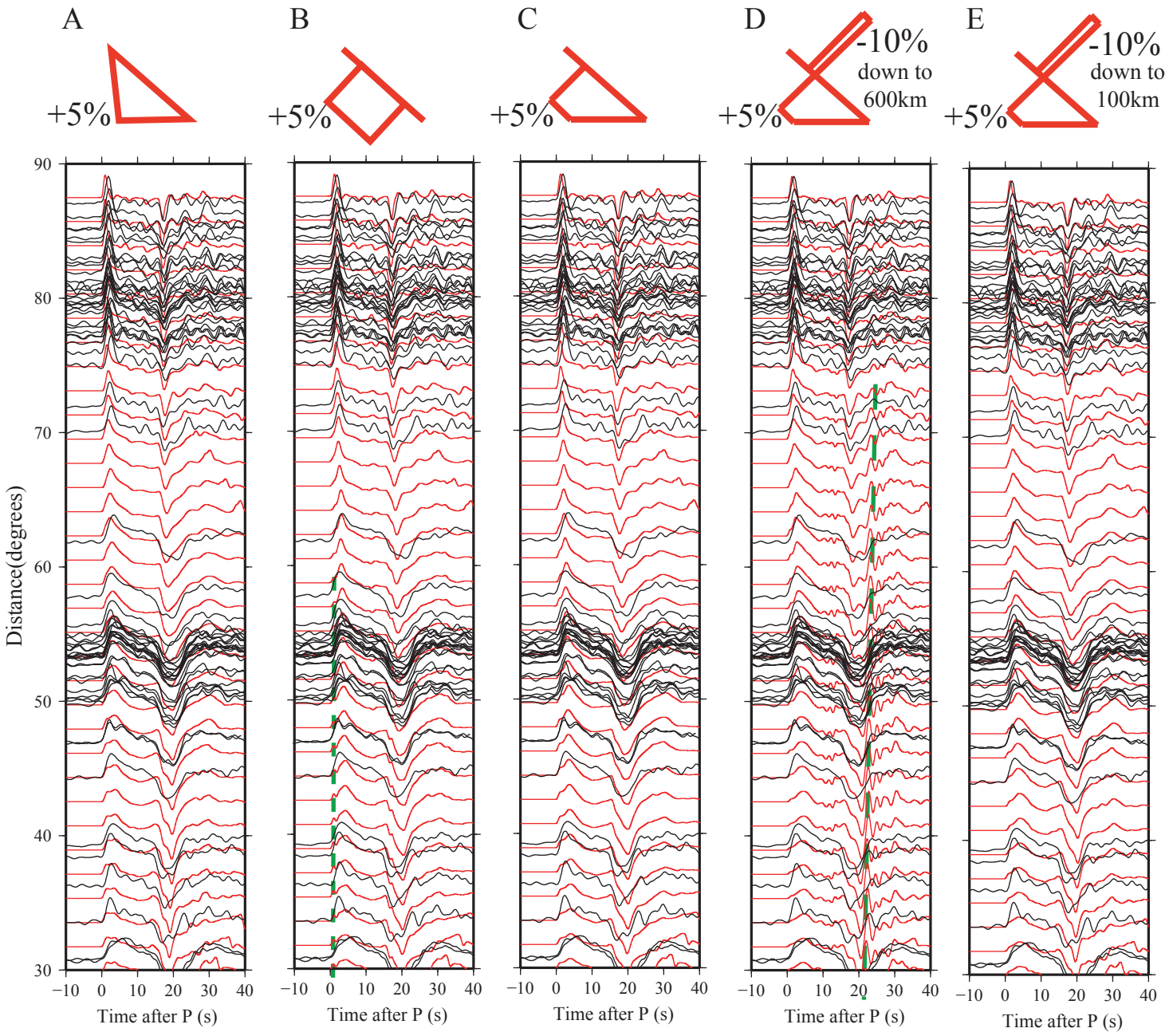

Figure S3. Test of waveform sensitivities to slab sharpness. For each panel, the observed seismograms are shown as black, and the synthetics using different velocity profiles across the slab (displayed on top) are in red. **(A)** preferred model, has smooth edge on each side, **(B)** has sharp edges on both sides, **(C)** has sharp top but smooth bottom. **(D)** and **(E)** are modified from (C) with a low-velocity layer on top, to 600 km and 100 km depths, respectively. In (B), the sharp edges on both sides produce distinct early arrivals (marked by the green dashed line), which are not observed in real data. These distinct arrivals due to the sharp slab are similar to the double pulses in the synthetic examples in Figure 1A and 1B. The slab model with sharp top in (C) provides similar waveform fits as the preferred model, therefore we cannot distinguish the models in (A) and (C) using the current dataset. We also test the teleseismic waveform sensitivity to the depth extent of LVZ using two end-member models, one with a 10 km thick, -10% LVZ down to 600 km depth, another with the same LVZ but only to 100 km depth, as shown in (D) and (E), respectively. In (D), the long LVZ serves as a strong wave-guide and produces strong high-frequency teleseismic coda waves in the synthetics (marked by the green dashed line), which are not observed in the real data. In contrast, the synthetics with LVZ down to 100 km fit the observations better in (E).

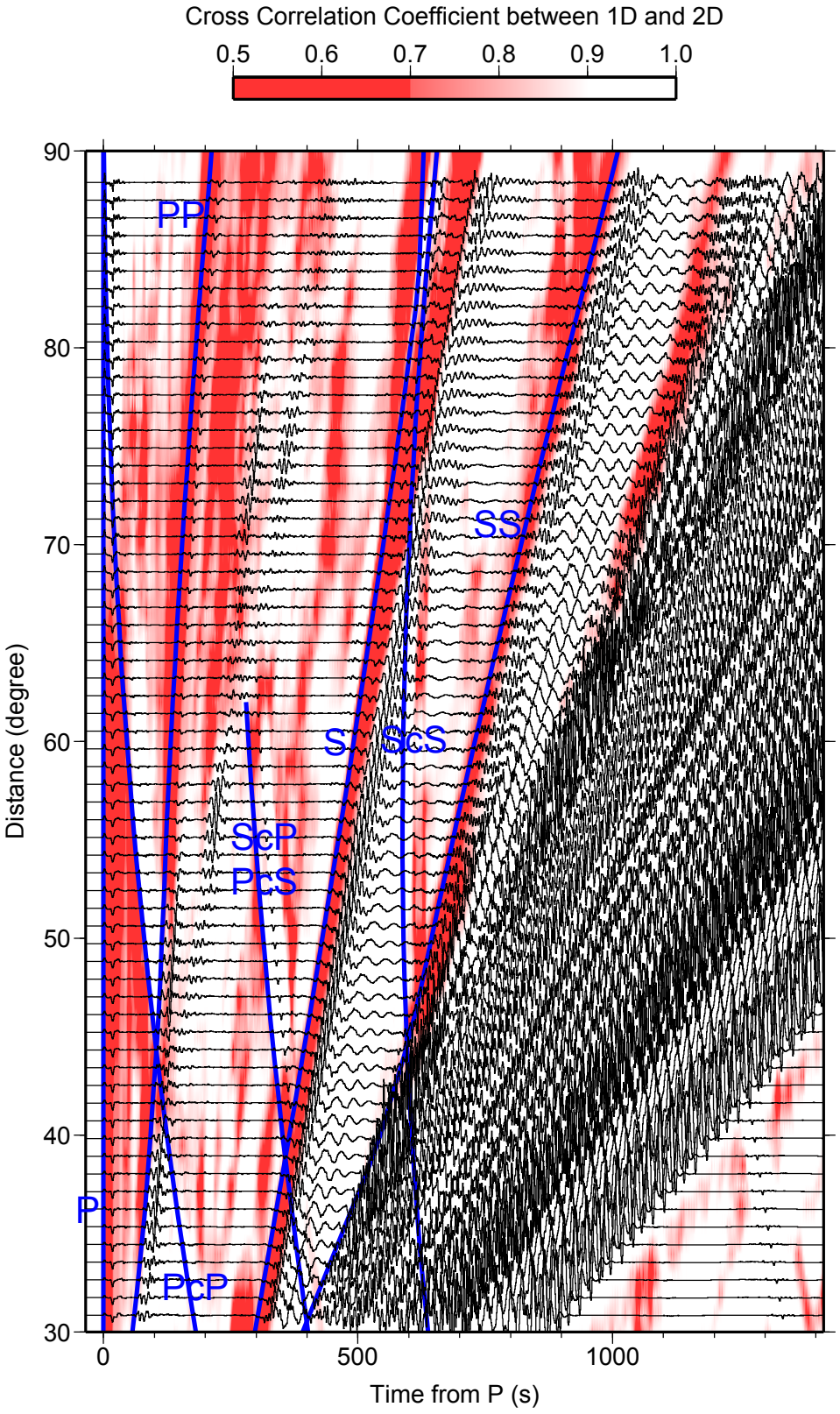

Figure S4. Complete synthetic record section of the 2009 earthquake with the preferred slab model. The blue lines mark the major teleseismic body wave phases. The later wave packages with largest amplitudes are the surface waves. To highlight the effect of the subducted slab, we compare the synthetic seismograms from models with/without the slab by moving-window cross-correlations. The background color shows the maximum cross-correlation coefficients allowing 5s shift. High cross-correlation (>0.9, white) means little waveform effect from slab, and low cross-correlation (<0.7, red color) highlights strongly distorted waveforms. Note that the surface waves with large amplitudes are not affected by the slab structure